Paleobiology, 45(1), 2019, pp. 182–200
DOI: 10.1017/pab.2018.48

PALEOBIOLOGY
A PUBLICATION OF THE Paleontological SOCIETY

The function(s) of bone ornamentation in the crocodylomorph osteoderms: a biomechanical model based on a finite element analysis

François Clarac, Florent Goussard, Vivian de Buffrénil, and Vittorio Sansalone

Abstract.—This paper aims at assessing the influence of the bone ornamentation and, specifically, the associated loss of bone mass on the mechanical response of the crocodylomorph osteoderms. To this end, we have performed three-dimensional (3D) modeling and a finite element analysis on a sample that includes both extant dry bones and well-preserved fossils tracing back to the Late Triassic. We simulated an external attack under various angles on the apical surface of each osteoderm and further repeated the simulation on an equivalent set of smoothed 3D-modeled osteoderms. The comparative results indicated that the presence of an apical sculpture has no significant influence on the von Mises stress distribution in the osteoderm volume, although it produces a slight increase in its numerical score. Moreover, performing parametric analyses, we showed that the Young's modulus of the osteoderm, which may vary depending on the bone porosity, the collagen fiber orientation, or the calcification density, has no impact on the von Mises stress distribution inside the osteoderm volume. As the crocodylomorph bone ornamentation is continuously remodeled by pit resorption and secondary bone deposition, we assume that the apical sculpture may be the outcome of a trade-off between the bone mechanical resistance and the involvement in physiological functions. These physiological functions are indeed based on the setup of a bone superficial vessel network and/or the recurrent release of mineral elements into the plasma: heat transfers during basking and respiratory acidosis buffering during prolonged apnea in neosuchians and teleosaurids; compensatory homeostasis in response to general calcium deficiencies. On a general morphological basis, the osteoderm geometric variability within our sample leads us to assess that the global osteoderm geometry (whether square or rectangular) does not influence the von Mises stress, whereas the presence of a dorsal keel would somewhat reduce the stress along the vertical axis.

François Clarac. Sorbonne Université, Centre National de la Recherche Scientifique, Institut des Sciences de la Terre de Paris, UMR 7193, 4 place Jussieu, BC 19-75005 Paris, France; and Département Histoire de la Terre, UMR 7207, Centre de Recherche en Paléontologie–Paris, Muséum National d'Histoire Naturelle/Centre National de la Recherche Scientifique /Sorbonne Université, Bâtiment de Géologie Paris Cedex 05, F-75231, France. E-mail: francois.clarac@mnhn.fr. Present address: Uppsala University, Department of Organismal Biology, Subdepartment of Evolution and Development, Norbyvägen 18A, SE-752 36, Uppsala, Sweden.

Florent Goussard. Département Histoire de la Terre, UMR 7207, Centre de Recherche en Paléontologie–Paris, Muséum National d'Histoire Naturelle/Centre National de la Recherche Scientifique/ Sorbonne Université, Bâtiment de Paléontologie Paris Cedex 05, F-75231, France. E-mail: florent.goussard@mnhn.fr

Vivian de Buffrénil. Département Histoire de la Terre, UMR 7207, Centre de Recherche en Paléontologie–Paris, Muséum National d'Histoire Naturelle/Centre National de la Recherche Scientifique/Sorbonne Université, Bâtiment de Géologie Paris Cedex 05, F-75231, France. E-mail: vivian.de-buffrenil@mnhn.fr

Vittorio Sansalone. Université Paris-Est, Laboratoire Modélisation et Simulation Multi Echelle, MSME UMR 8208 CNRS, 61 avenue du Général de Gaulle, 94010 Créteil Cedex, France. E-mail: vittorio.sansalone@u-pec.fr

Accepted: 11 December 2018
Data available from the Dryad Digital Repository: https://doi.org/10.5061/dryad.5qb8387

Introduction

Among the different bones that compose the vertebrate skeleton, the osteoderms (when present) are set up through an integumentary ossification of the dermis (Gilbert et al. 2001; Vickaryous and Hall 2008; Vickaryous and Sire 2009). This mechanism may be initiated in part by endothelial cell precursors that undergo endothelial-to-mesenchymal transition and further acquire an osteoblast phenotype (Dubansky and Dubansky 2018). As the osteoderms occupy an outer position along the postcranial region, the functional role of these bony elements is often claimed to be involved in defense against impinged loads (Sun and Chen 2013; Chen et al. 2014; Broeckhoven et al. 2015; Du Plessis et al. 2018). Even though this implication seems obvious when the osteoderms form a continuous shield, as in the

© 2019 The Paleontological Society. All rights reserved. 0094-8373/19

https://doi.org/10.1017/pab.2018.48 Published online by Cambridge University Press

turtles (Acrai and Wagner 2013; Chen et al. 2015), xenarthrans (Vickaryous and Hall 2006; Chen et al. 2011; Wolf et al. 2012), ankylosaurs (Scheyer and Sander 2004), aetosaurs (Cerda and Desojo 2011), squamates (Anguidae; Zylberberg and Castanet 1985; Anjan and Bhullar 2008; Bochaton et al. 2013), "armored fishes" (Yang et al. 2013a, 2013b), and crocodilians (Trutnau and Sommerlad 2006), it is more controversial in some other taxa in which the osteoderms consist of a few anterior–posterior rows: chondrosteans (Burdak 1986), the early crocodylomorphs (Nesbitt 2011; Irmis et al. 2013), and thyreophoran dinosaurs (Main et al. 2005). In this regard, because the osteoderms provide a vascular proliferation in the dermis (Clarac et al. 2018), it has been assumed that these bones may also be involved in different physiological functions, such as the acidosis buffering during apnea in semiaquatic taxa (turtles and crocodilians; Jackson and Heisler 1982; Jackson 2000; Jackson et al. 1999, 2000a, 2000b, 2003) and heat exchanges in both large ectothermic vertebrates (crocodilians) and ornithischian dinosaurs (Seidel 1979; Farlow et al. 2010). Nonetheless, because the dermal bones (both the dermatocranium—i.e., the part of the skull composed of dermal bones—and the osteoderms) usually show a pronounced superficial ornamentation (a repetitive pattern often made of pits separated by ridges; Bystrow 1935; Iordansky 1973; Scheyer et al. 2007, 2012; Burns et al. 2013) within most taxa that present a well-developed integumentary shield (mentioned earlier), it has been proposed that this feature may play a role in dermal bone mechanical resistance by modifying the stress distribution, as its presence changes the surface, the volume, and, consequently, the mass of the bone (Coldiron 1974; Rinehart and Lucas 2013). Therefore, because the crocodilian osteoderms show a well-developed bone ornamentation (made of resorbed pits and grooves; Buffrénil 1982; Buffrénil et al. 2015), they consequently present a good model to test whether the presence of bone ornamentation modifies the dermal bone strengthening. Moreover, among Pseudosuchia (crocodylomorphs and their close relatives) there exist a wide diversity of osteoderm morphological patterns, as these bony plates may be isolated as well as either juxtaposed or articulated in longitudinal rows (Ross and Mayer 1983; Burns et al. 2013). Each individual osteoderm happens to present a dorsal keel or a spike and a variable degree of ornamental pit excavation (Clarac et al. 2015). For instance, there are two dorsal columns of paramedian osteoderms running from the back of the head along the midline of the body, showing either a radiating or vertical pitted shallow sculpture pattern in the protosuchids and erpetosuchids (Kälin 1955; Benton and Walker 2002), whereas there are more than two dorsal columns of paramedian and lateral articulating osteoderms that form a dorsal (sometimes also ventral) carapace in Aetosauria (Long and Ballew 1985; Heckert et al. 2017; Desojo et al. 2013; Schoch and Desojo 2016). In phytosaurs, which are either considered as pseudosuchians or as the archosaurs' sister taxon (Nesbitt 2011), the dorsal surface is covered with multiple diamond-shaped or roughly triangular osteoderms arranged in two paramedian rows. Those osteoderms often have a dorsal surface that is covered with patterns of ridges and grooves surrounding a central keel. Additional osteoderms loosely cover the appendicular skeleton, as in some extant crocodilians (Ross and Mayer 1983), while the phytosaurs present a unique structure among archosauriforms: multiple osteoderms overlapping and interlocking under the throat, the so-called gular shield (Stocker and Butler 2013; Scheyer et al. 2014).

The main purpose of this paper is therefore to test whether the apical ornamentation may play a role in terms of load-bearing capacity and mechanical strength of the osteoderm. To this end, we used numerical modeling and simulation to investigate the stress distribution induced in the osteoderm by a predator attack. The effect of the ornamentation was thus assessed by comparing the results obtained on three-dimensional (3D) models of actual (ornamented) and smoothed (nonornamented) osteoderms.

In the following section we will describe the samples considered in this study and the numerical models developed. Then we will present qualitative and quantitative results obtained through our numerical simulations for both actual and smoothed osteoderms.

https://doi.org/10.1017/pab.2018.48 Published online by Cambridge University Press

The last section will be devoted to discussing and comparing these results and to drawing some conclusions on the mechanical effects of the ornamentation in order to decipher its functional implication(s) (at least in Crocodylomorpha).

Material and Methods

Biological Sampling.—The sample includes five crocodylomorph osteoderms and one aetosaur osteoderm (Table 1). They include either dry bones from extant species (i.e., *Osteolaemus tetraspis*, *Caiman crocodilus*) or well-preserved fossils that trace back to the Triassic or later periods (i.e., *Aetosaurus* sp., *Sarcosuchus imperator*, *Hyposaurus rogersii*). We included two osteoderms from *O. tetraspis* in order to consider the intraspecific variability within this interspecific sample. The full set of osteoderms thus represents five different taxa showing both various global morphologies and a well-developed bone ornamentation, so the resulting analysis consists of a model that can be generalized to Crocodylomorpha. The *O. tetraspis* and *C. crocodilus* osteoderms possess a central longitudinal keel and come from the nuchal region, whereas the three other specimens are flatter and come from the dorsal shield, as they possess an articular shelf. Unlike the *H.rogersii* osteoderm, which is fully flat, the *S.imperator* osteoderm shows a keel that does not modify the osteoderm global flat shape, as its position is lateral (Sereno et al. 2001). The *Aetosaurus* sp. osteoderm also is unique in presenting an apical spike consisting of a local protuberance that is medial to the osteoderm midpoint and close to the posterior margin, thus also not modifying the osteoderm global flat morphology (Cerda and Desojo 2011). Although we did not perform histological cross sections on our sample, we assume that all the collected osteoderm specimens possess a diploe structure (i.e., they are made up of an outer shell of compact bone embedding a core of trabecular bone), because several authors reported such a histological structure in both the neosuchian (Buffrénil et al. 2015) and the aetosaur osteoderms (Cerda and Desojo 2011; Desojo et al. 2013; Scheyer et al. 2014). Indeed, these bones consist of the superposition of three layers: a basal layer that is usually lamellar or parallel fibered, a midlayer that is cancellous and includes both primary and secondary osteons, and an apical layer made of lamellar or parallel-fibered bone that is remodeled by pit resorption and secondary bone deposit.

All the specimens were directly sampled in museum collections: the MNHN comparative anatomy and paleontology collections (Muséum National d'Histoire Naturelle, Paris, France) and the AMNH paleontology collections (American Museum of Natural History, New York, USA) (see Table 1).

Three-Dimensional Modeling.—The 3D models of the osteoderms were created using the procedure described in Clarac et al. (2017a) and outlined here. The four osteoderms from the MNHN collections were scanned with a Breuckmann StereoScan 3D-surface scanner, a device that reconstructs 3D objects using phase contrast. The bone surface is virtually reconstructed as a mesh of adjacent polygons, folded according to bone reliefs inside a 3D space. We used two scope ranges, depending on sample size, to obtain adequate mesh resolutions: a small scope range (60 mm) with a resolution of 12 μm and a medium scope range (250 mm) with a resolution of 18 μm. The four 3D objects thus obtained were exported into Polygon File Format (PLY format). Imperfections of the mesh (noise, artifacts, self-interactions, etc.), when present, were corrected using Geomagic Studio 2012 cleaning tools (Geomagic Worldwide Headquarters, 430 Davis Drive, Marisville, N.C. 27560, USA). The two osteoderms from the AMNH paleontology collection were reconstructed in three dimensions using photogrammetry. Therefore, we used a portable camera for taking a series of photographs of the two osteoderms under various angles under controlled and repeatable conditions. For this purpose, the camera was fixed on a stage and pointed toward the osteoderm (target), which was left rotated to mimic the process used with the StereoScan 3D-surface scanner. We used a Canon 60D camera equipped with a Canon 60 mm/2 macro objective and a Canon Speedlite 320EX flash. Camera parameters were set to get clear photographs (sensitivity: 100 ISO, objective aperture: 16, exposure time: automatic). Each

https://doi.org/10.1017/pab.2018.48 Published online by Cambridge University Press

TABLE 1. Sampled specimens with taxonomic references.

Family	Genus	Species	Collection number	Author	Year	Period
Alligatoridae	*Caiman*	*crocodilus*	MNHN-1989-6489	Linnaeus	1758	Extant
Crocodylidae	*Osteolaemus*	*tetraspis*	MNHN-AC.1991.4488a	Cope	1861	Extant
Crocodylidae	*Osteolaemus*	*tetraspis*	MNHN-AC.1991.4488b	Cope	1861	Extant
Pholidosauridae	*Sarcosuchus*	*imperator*	MNHN-1966-15 Gad-4	Broin & Taquet	1966	Cretaceous
Dyrosauridae	*Hyposaurus*	*rogersii*	AMNH-2389	Owen	1849	Cretaceous
Aetosauridae	*Aetosaurus*	sp.	AMNH-19331	Fraas	1877	Triassic

osteoderm was laid on one edge on a rotating pad that was centered on a fixed 360° graduated plastic sheet. Each specimen was then photographed every 10° while rotating along a 36-photograph series. The distance between the camera and the osteoderm was set so that the osteoderm completely filled the camera field of view. The 3D model was generated automatically for each specimen after uploading the 36 pictures in JPEG format (Agisoft Photoscan Professional v. 1.1.4). This process involves four consecutive stages: aligning pictures, creating a dense cloud, meshworking, and building a surface texture. Pictures partially blurred by short field depth were manually deleted as all pictures were previously checked during an individual review of each picture before the automatic alignment. Finally, 3D models were exported in PLY format. It is worth noting that all the 3D models obtained using either Breuckmann surface scanner or photogrammetry have similar accuracy (Clarac et al. 2017a).

As our aim was to assess the effect of ornamentation on the mechanical response of the osteoderms, we duplicated each 3D-reconstructed osteoderm to create a copy without ornamentation. Because the ornamentation in our samples is known to result from osteoclastic bone resorption on the apical surface (Buffrénil 1982; Buffrénil et al. 2015), this comparative model was set up by suppressing all the pits and replacing the ornamented apical surface with a smooth envelope (using Geomagic Studio 12; for more details, see Clarac et al. 2017b).

Moreover, to remove the size differential of the osteoderms (which ranged in size from a few centimeters to a few tens of centimeters), in our comparative analysis, we rescaled all the samples so that they have the same ornamented surface area (OSA). We first measured the area of the apical, ornamented surface of all the osteoderms using the Compute Selected Area tool in Geomagic Studio 12. Then, after selecting a reference sample (*C. crocodilus*, MNHN-1989-6489), for each osteoderm, we computed a linear scale factor as the square root of the ratio between the reference OSA and its own OSA (the square root is needed, because this linear scale factor is based on measures of area).

Each linear scale factor was used to rescale the corresponding specimen with respect to its centroid (by means of the function *model change* in Geomagic Studio 12). The result of this operation was the acquisition of a set of six osteoderms having their original shape but the same OSA value. The same scale factors were used on the corresponding smoothed osteoderms. It should be noted that the surface scanner preserves the actual dimensions when generating the PLY files, whereas photogrammetry does not. This is not a limitation; the actual size of the osteoderms does not matter with respect to this study, because all the osteoderms, whatever their actual size, are rescaled to have the same OSA value. Therefore, the scaling factors used to rescale the 3D models in Geomagic refer to the actual size of the osteoderms of the MNHN collection and to a fictitious size arbitrarily set by Geomagic Studio 12 while importing the PLY files for those coming from the AMNH collection. The actual scaling factors of these latter specimens can be only estimated. The actual scale factors of the MNHN samples and the estimated scale factors of the AMNH samples are reported in Table 2.

Eventually, for sake of limiting the computational time needed for the subsequent finite element analysis (FEA), we simplified the

https://doi.org/10.1017/pab.2018.48 Published online by Cambridge University Press

TABLE 2. Sampled osteoderms with morphometric data. The ΔMass is calculated assuming a bone density of 2g/cm^3. *Estimated scale factor based on the osteoderm real size (different from the value used for scaling the 3D model in Geomagic Studio). *Osteolaemus tetraspis* (a),MNHN-AC.1991.4488a; (b), MNHN-AC.1991.4488b.

Species	Shape	Scaled dimensions ($L_y/L_x/L_z$) mm	Linear scale factor	Scaled volume (ornamented) mm^3	Scaled volume (smoothed) mm^3	ΔVolume mm^3	ΔMass mg	*LV* %
Caiman crocodilus	Keeled rectangular	27.8/18.2/4.6	1	800	855	55	110	6.5
Osteolaemus tetraspis (a)	Keeled square	23.2/24.3/3.5	1.74	878	992	114	228	11.5
Osteolaemus tetraspis (b)	Keeled square	26.2/24.8/3.6	1.83	939	1050	111	222	10.6
Sarcosuchus imperator	Flat rectangular	14.4/32.7/2.1	0.13	602	643	41	82	6.4
Hyposaurus rogersii	Flat rectangular	17.5/26.0/3.0	0.5*	654	754	100	200	13.3
Aetosaurus sp.	Spiked reactangular	13.2/40.2/4.4	0.2*	595	659	64	128	9.7

surface representation of our 3D models and reduced the number of surface triangles to between 20,000 and 30,000 using the remeshing tools of Geomagic Studio 12 (detailed in Supplementary Fig. 1). These surface meshes are adequate with respect to the studied specimens (size and morphology).

Finite Element Analysis.—The 3D models of osteoderms were uploaded into Comsol software (COMSOL Multiphysics v. 5.2, COMSOL AB, Stockholm, Sweden) to perform an FEA simulating the attack of a predator. The element size of the finite element (FE) mesh was fixed to ensure convergence of the relevant mechanical parameters (average von Mises stress and high-stress regions—see below; Supplementary Fig. 2).

A comparative analysis was performed on ornamented and smoothed models of osteoderms, looking at the distribution of the von Mises stress—a scalar measure encompassing the whole 3D stress state, which is commonly used to define a strength criterion in terms of the maximum distortion of a ductile material (yield strength; von Mises 1913). Moreover, a sensitivity analysis was also performed with respect to several modeling parameters.

The osteoderms were assumed to be made of a homogeneous, isotropic, linearly elastic material characterized by Young's modulus (E_o) and the Poisson ratio (ν_o). Young's modulus (E_o) characterizes the stiffness (i.e., the resistance to deformation of the osteoderm), and its value was arbitrarily set to 10 GPa, which is on the order of the elastic modulus of alligator osteoderms obtained through nanoindentation tests (Sun and Chen 2013). Indeed, this value depends on the specific microstructural features of the osteoderm, namely, bone porosity and collagen fiber orientation (Sun and Chen 2013). As outlined by previous authors (Scheyer and Desojo 2011; Burns et al. 2013; Cerda et al. 2013; Buffrénil et al. 2015), the crocodylomorph osteoderms show a variable porosity and are composed not only of compact bone but also show a diploe structure (at least in the modern forms). Moreover, microcrack orientation can introduce some anisotropy in the elastic moduli of the osteoderm (Chen et al. 2014). In view of the uncertainty affecting the actual value of E_o,

https://doi.org/10.1017/pab.2018.48 Published online by Cambridge University Press

we performed a parametric analysis in *C. crocodilus* to estimate the effects of the variation of the Young's modulus of the osteoderm. As no experimental measures exist for the value of the Poisson ratio of the osteoderms, we set $\nu_o = 0.18$, which is typical of compact bovine femoral bone (Pithioux et al. 2002).

The attack of a predator was modeled by applying a force, $F = 1000$ N, orthogonal to the apical surface of each specimen (above the centroid). This value is an approximation of a *C. crocodilus* molariform bite force (F_{tot}; following Erickson et al. 2012), which simulates an external attack in an intraspecific fight or in a predator ambush, such as might be produced by a jaguar claw (*Panthera onca*; Da Silveira et al. 2010; Azevedo and Verdade 2011). Different angles of attack were considered, parameterized by the pair of angular coordinates (α, λ) depicted in Figure 1A. The orientation of the force was initially set in the vertical direction (z-axis, $\alpha = 0°$), then the force direction was tilted at an angle $\alpha = \pm 45°$ toward either the transversal axis x ($\lambda = 0°$) or the longitudinal axis y ($\lambda = 90°$), as an attack (whether a bite or a claw) may come from different directions (see Fig. 1A). Thus, components of the force read: $F_x = F \sin(\alpha) \cos(\lambda)$, $F_y = F \sin(\alpha) \sin(\lambda)$, and $F_z = F \cos(\alpha)$. Overall, five loading conditions were considered whose angular coordinates are depicted in Figure 1A.

The FE mesh and the other boundary conditions (BCs) are shown in Figure 1B. The geometry was meshed using the built-in meshing tools of COMSOL software, resulting in about 10^5 tetrahedral elements. Quadratic polynomial shape functions were used in each element to locally interpolate the displacement field. Besides the bite force, we applied BCs on the osteoderm that simulated its actual configuration in vivo. Because each osteoderm is connected to its neighbors along its four lateral edges within the dorsal shield (Sun and Chen 2013), we applied distributed springs on its lateral boundaries. Spring stiffness was estimated as $K_x = E_o/(N_x \cdot L_x)$ for the springs acting along the transversal axis (x direction; red spring in Fig. 1B), where N_x is the number of neighboring osteoderms and L_x is the typical dimension of the osteoderm in the x direction. K_x has the physical dimensions of $[N/L^2 \cdot L]$

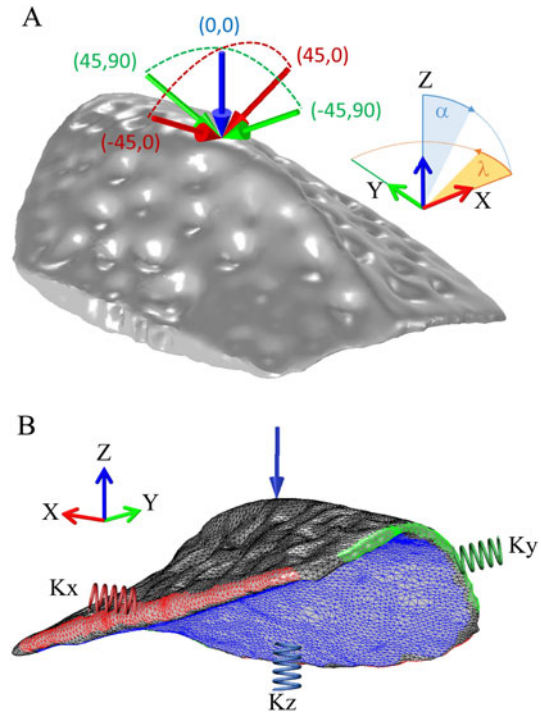


FIGURE 1. A, Geometry and forces applied on a typical osteoderm (*Caiman crocodilus*) to simulate a bite coming from different directions. The force direction is parameterized by the pair of angles (α, λ). The five loading conditions considered in this study are depicted, and their angular coordinates are expressed in degrees. B, Finite element mesh and boundary conditions of a typical osteoderm (*C. crocodilus*). Elastic springs are applied on the lateral (red and green) and basal (blue) sides of the osteoderm (see text for details). X, transversal axis; Y, longitudinal axis; Z, vertical axis.

and represents the force per unit area needed to produce a unit displacement. Similarly, the stiffness of the springs acting along the longitudinal axis (y direction; green spring in Fig. 1B) was estimated as $K_y = E_o/(N_y \cdot L_y)$. The values of L_x and L_y of all the osteoderms can be found in Table 2. N_x and N_y are free parameters of the model. Numerical results for all osteoderms were computed by setting $N_x = N_y = 1$. However, we performed a parametric study in *C. crocodilus* by considering up to five neighboring osteoderms in each direction to assess the influence of the osteoderm locality on the experimental stress (Supplementary Fig. 3). Because the dorsal shield is carried by the axial musculature (Gasc 1981), we applied distributed elastic springs on the basal side of the osteoderm, whose stiffness was estimated as

https://doi.org/10.1017/pab.2018.48 Published online by Cambridge University Press

$K_z = E_b/L_z$, where E_b and L_z are the Young's modulus and thickness of the basal soft tissue, respectively. These two parameters are quite hard to identify. We arbitrarily set $E_b =$ 100 MPa (slightly smaller than the Young's modulus of the muscles measured in tensile conditions; McKee et al. 2011) and $L_z = 1$ cm (typical distance between the osteoderm and the underlying skeletal structure) in our simulations. As the value of E_b can span several orders of magnitude according to the specific tissue (Akhtar et al. 2011; McKee et al. 2011; Kot 2012), we performed a parametric study in *C. crocodilus* by varying E_b from 0.1 to 1000 MPa.

Quantitative Assessment of the Bone Ornamentation.—In this study, our aim is to investigate the mechanical effects of the loss of bony mass due to the ornamentation of the osteoderms. First, from a mechanical point of view, comparison between ornamented and smoothed osteoderms is made in both qualitative and quantitative terms with respect to the von Mises stress. Qualitative comparison is made looking at the distribution of von Mises stress in the osteoderm. Quantitative comparison is made by means of suitable stress-related indexes, namely: (1) the *average* von Mises stress $\bar{\sigma}_{VM}$ in the osteoderm:

$$\bar{\sigma}_{\mathrm{VM}} = \frac{1}{\mathrm{V_o}} \int_{\mathrm{V_o}} \sigma_{\mathrm{VM}} dV, \qquad (1)$$

where σ_{VM} is the von Mises stress, and V_o is the volume of the osteoderm; and (2) the *high-stress volume fraction* VF_i, that is, the ratio between the volume V_i of the osteoderm where the von Mises stress exceeds a fixed threshold σ_i and the whole volume of the osteoderm:

$$V_i = \int_{V_o} 1_{\sigma_{VM} > \sigma_i} dV, \; VF_i = V_i/V_o \qquad (2)$$

where $1_{\sigma_{VM} > \sigma_i}$ is the characteristic function taking value 1 in the regions where σ_{VM} exceeds σ_i and 0 elsewhere. Two thresholds were fixed in this study, namely, $\sigma_1 = 100$ MPa (which roughly corresponds to the strength of compact bone) and $\sigma_2 = \sigma_1/2$; the corresponding high-stress volume fractions are thus denoted VF_1 and VF_2, respectively.

Second, from a morphological point of view, comparison between ornamented and smoothed osteoderms is made by looking at the mass loss due to ornamentation, which is excavated by pit resorption in the apical cortex of the osteoderms. This mass quantification is followed by the loss of volume, as the bone density in the peripheral cortex (compact bone) may be considered constant (2 g/cm^3; after Blanton and Biggs 1968). Herein, quantifying the loss of volume due to ornamentation entails first measuring the volume within the ornamented osteoderm before repeating the operation on a smoothed copy. This process results in the acquisition of a variable that defines the loss of bone volume of the smoothed osteoderm due to the excavation of the pits on its apical surface (expressed as a percentage; Clarac et al. 2017b):

$$LV = 100\left(\frac{SoV - RoV}{SoV}\right), \qquad (3)$$

where *SoV* and *RoV* are the "smoothed osteoderm volume" and "real osteoderm volume," respectively. Table 2 presents all the relevant morphometric data of ornamented and smoothed osteoderms.

Results

Parametric Analysis in Caiman crocodilus.—Figure 2A shows the von Mises stress in the *C. crocodilus* osteoderm (on the left) and the high-stress regions (on the right) where the von Mises stress exceeds the stress thresholds σ_1 in dark gray (blue online) and σ_2 in light gray (purple online), as a function of the Young's modulus of the osteoderm (E_o). The same results are shown in Figure 2B as a function of the Young's modulus of the basal tissue (E_b). Qualitatively, the stress distribution in the osteoderm is not affected noticeably by the value of E_o. By contrast, E_b does affect the stress distribution in the osteoderm, smaller values of E_b being associated with higher stress.

The parametric analysis shows that both the average von Mises stress ($\bar{\sigma}_{VM}$) and the

https://doi.org/10.1017/pab.2018.48 Published online by Cambridge University Press

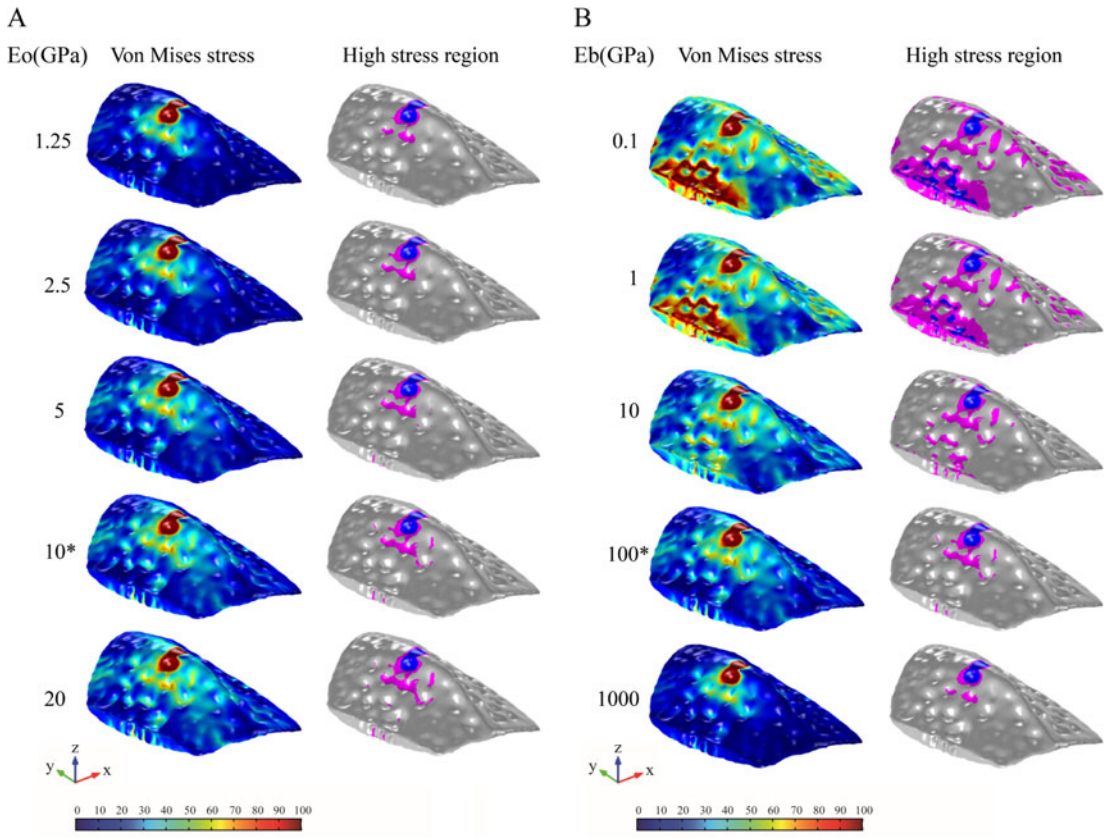


FIGURE 2. A, Parametric analysis with respect to the Young's modulus of the osteoderm (E_o). Left: von Mises stress; color scale: 0 (blue; light gray) to 100 MPa (red; dark gray). Right: High-stress volume fractions VF_1 (blue; dark gray) and VF_2 (purple; light gray) as a function of the Young's modulus of the osteoderm (E_o). Relevant reference parameters are: E_b = 0.1 GPa (Young's modulus of the basal tissue); $N = 1$ (number of lateral osteoderms); and $\alpha, \lambda = 0°$ (force orientation). An asterisk (*) denotes the reference value of E_o. B, Parametric analysis with respect to the Young's modulus of the basal tissue (E_b). Left: von Mises stress; color scale: 0 (blue; light gray) to 100 MPa (red; dark gray). Right: High-stress volume fractions: VF_1 (blue; dark gray) and VF_2 (purple; light gray) as a function of the Young's modulus of the basal tissue (E_b). Relevant reference parameters are: $E_o = 10$ GPa (Young's modulus of the osteoderm); $N = 1$ (number of lateral osteoderms); and $\alpha, \lambda = 0°$ (force orientation). An asterisk (*) denotes the reference value of E_b, which was used for the simulation on the full sample (presented in Table 1).

high-stress volume fractions (VF_1 and VF_2) increase as the Young's modulus E_o of the osteoderm increases (Fig. 3A,B). Conversely, both the average von Mises stress and the high-stress volumes of the osteoderm decrease as the Young's modulus E_b of the basal tissue increases (Fig. 3C,D). Both E_o and E_b strongly affect the average von Mises stress (Fig. 3A,C). Moreover, whereas E_o has a small or negligible effect on the volume fractions VF_1 (blue/dark gray lines in Fig. 3B) and VF_2 (purple/light gray lines in Fig. 3B), E_b does affect the values of VF_1 and VF_2 (blue/dark gray and purple/light gray lines in Fig. 3D, respectively).

The parametric analysis with respect to the number of lateral osteoderms ($N = N_x = N_y$) has shown that this parameter has a negligible effect (differences of a few percent) on both the average von Mises stress $\bar{\sigma}_{VM}$ and the high-stress volume fractions VF_1 and VF_2 as N increases from 1 to 5 (Supplementary Fig. 3).

The Influence of the Osteoderm Global Morphology on the Mechanical Resistance.—We performed a principal component analysis (PCA; Fig. 4) using $\bar{\sigma}_{VM}$ and VF_1 and VF_2 scores on the full set of the ornamented osteoderms (Table 3). The main component (PC 1) explains 94% of the variance and is positively correlated

https://doi.org/10.1017/pab.2018.48 Published online by Cambridge University Press

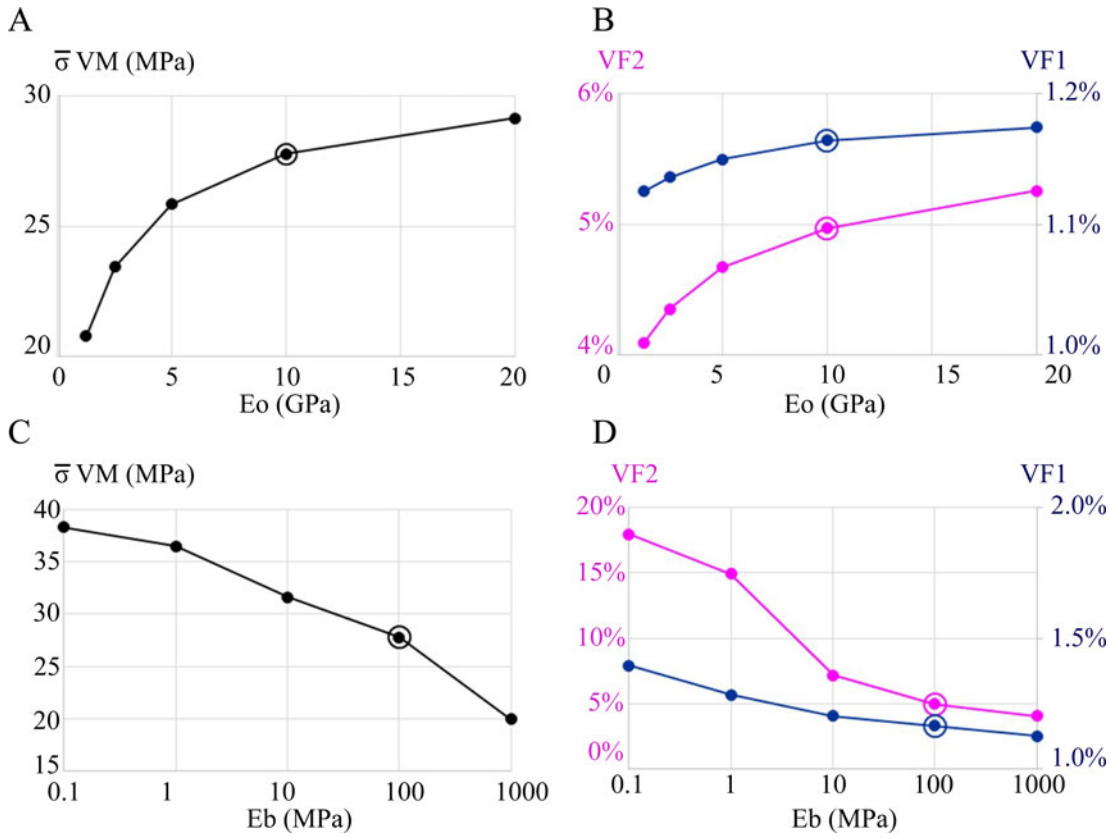


FIGURE 3. Parametric analysis in *Caiman crocodilus* with respect to the Young's modulus of the osteoderm (E_o; A, B) and of its basal tissue (E_b; C, D). A, Average von Mises stress in the osteoderm as a function of the Young's modulus of the osteoderm (E_o). B, High-stress volume fractions VF_1 (blue/dark gray line; right-side scale) and VF_2 (purple/light gray line; left-side scale) as a function of the Young's modulus of the osteoderm (E_o). Relevant reference parameters are: $E_b = 0.1$ GPa (Young's modulus of the basal tissue); $N = 1$ (number of lateral osteoderms); and $\alpha, \lambda = 0°$ (force orientation). C, Average von Mises stress in the osteoderm as a function of the Young's modulus of the basal tissue (E_b). D, High-stress volume fractions VF_1 (blue/dark gray line; right-side scale) and VF_2 (purple/light gray line; left-side scale) as a function of the Young's modulus of the basal tissue (E_b). Relevant reference parameters are: $E_o = 10$ GPa (Young's modulus of the osteoderm); $N = 1$ (number of lateral osteoderms); and $\alpha, \lambda = 0°$ (force orientation). See text for details.

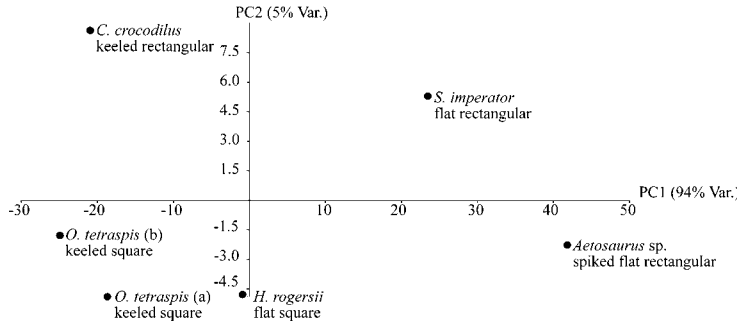


FIGURE 4. Principal component analysis of the sampled osteoderm stress variables: VF_1, VF_2, $\bar{\sigma}_{VM}$ with variation of α (0°, 45°, –45°) and λ (0°, 90°, –90°); *PC1* explains 94% of the variance, 5% of the variance is explained by *PC2*. Performed using PAST v. 2.17c (Hammer et al. 2001).

https://doi.org/10.1017/pab.2018.48 Published online by Cambridge University Press

TABLE 3. Mechanical indexes quantifying the von Mises stress distribution in the ornamented and smoothed specimens for each loading condition (α, λ) and in the average. $\bar{\sigma}_{VM}$, average von Mises stress in the osteoderm; VF_1 and VF_2, volume fractions of the regions where the von Mises stress exceeds the stress thresholds σ_1 and σ_2, respectively. See text for details. *Osteolaemus tetraspis* (a), MNHN-AC.1991.4488a; (b), MNHN-AC.1991.4488b.

Caiman crocodilus		Ornamented			Smoothed		
λ (°)	α (°)	$\bar{\sigma}_{VM}$ (MPa)	VF_1 (–)	VF_2 (–)	$\bar{\sigma}_{VM}$ (MPa)	VF_1 (–)	VF_2 (–)
0	0	27.77	1.2%	5.0%	25.18	1.0%	4.0%
0	−45	32.89	2.7%	13.7%	29.48	1.9%	9.9%
0	45	30.24	2.3%	12.6%	27.12	1.9%	9.6%
90	−45	25.96	1.4%	6.9%	23.05	1.2%	6.5%
90	45	27.31	1.4%	7.1%	25.61	1.2%	5.5%
Average		28.84	1.8%	9.1%	26.09	1.4%	7.1%
Osteolaemus tetraspis (a)		Ornamented			Smoothed		
λ (°)	α (°)	$\bar{\sigma}_{VM}$ (MPa)	VF_1 (–)	VF_2 (–)	$\bar{\sigma}_{VM}$ (MPa)	VF_1 (–)	VF_2 (–)
0	0	30.02	2.6%	14.0%	24.69	1.0%	7.7%
0	−45	24.44	1.6%	8.6%	21.22	1.0%	5.3%
0	45	29.65	3.2%	13.3%	22.69	1.1%	5.7%
90	−45	27.14	1.7%	9.9%	22.38	1.0%	5.3%
90	45	26.87	1.9%	9.6%	21.82	1.1%	4.8%
Average		27.63	2.2%	11.1%	22.56	1.0%	5.8%
Osteolaemus tetraspis (b)		Ornamented			Smoothed		
λ (°)	α (°)	$\bar{\sigma}_{VM}$ (MPa)	VF_1 (–)	VF_2 (–)	$\bar{\sigma}_{VM}$ (MPa)	VF_1 (–)	VF_2 (–)
0	0	28.01	1.6%	10.6%	25.50	1.0%	8.1%
0	−45	26.13	1.9%	9.7%	23.00	1.2%	6.7%
0	45	26.11	1.9%	8.8%	23.27	1.1%	6.5%
90	−45	26.06	1.9%	7.7%	22.92	1.1%	5.9%
90	45	24.18	1.3%	6.5%	21.87	1.0%	4.7%
Average		26.10	1.7%	8.6%	23.31	1.1%	6.4%
Sarcosuchus imperator		Ornamented			Smoothed		
λ (°)	α (°)	$\bar{\sigma}_{VM}$ (MPa)	VF_1 (–)	VF_2 (–)	$\bar{\sigma}_{VM}$ (MPa)	VF_1 (–)	VF_2 (–)
0	0	43.40	8.8%	25.2%	39.50	7.8%	22.9%
0	−45	46.07	6.9%	25.6%	42.30	6.0%	23.3%
0	45	39.32	5.5%	26.4%	35.22	4.8%	21.8%
90	−45	36.40	6.1%	20.2%	32.89	5.0%	17.6%
90	45	39.02	6.4%	21.9%	36.06	5.5%	20.2%
Average		40.84	6.8%	23.8%	37.20	5.8%	21.2%
Hyposaurus rogersii		Ornamented			Smoothed		
λ (°)	α (°)	$\bar{\sigma}_{VM}$ (MPa)	VF_1 (–)	VF_2 (–)	$\bar{\sigma}_{VM}$ (MPa)	VF_1 (–)	VF_2 (–)
0	0	37.10	5.5%	20.1%	29.37	2.8%	14.9%
0	−45	32.32	3.1%	15.2%	25.81	1.5%	9.5%
0	45	31.95	3.4%	14.4%	26.04	1.6%	9.6%
90	−45	34.00	3.6%	16.4%	27.98	1.8%	12.1%
90	45	32.32	3.1%	14.2%	26.24	1.5%	9.5%
Average		33.54	3.7%	16.1%	27.09	1.8%	11.1%
Aetosaurus sp.		Ornamented			Smoothed		
λ (°)	α (°)	$\bar{\sigma}_{VM}$ (MPa)	VF_1 (–)	VF_2 (–)	$\bar{\sigma}_{VM}$ (MPa)	VF_1 (–)	VF_2 (–)
0	0	52.51	12.2%	34.4%	45.53	9.0%	30.3%
0	−45	47.00	8.1%	29.8%	40.06	5.4%	25.0%
0	45	46.11	7.9%	28.1%	40.54	6.1%	24.0%
90	−45	44.11	7.9%	28.9%	38.64	6.3%	25.2%
90	45	41.72	7.8%	25.1%	36.02	6.0%	20.5%
Average		46.29	8.8%	29.3%	40.16	6.6%	25.0%

https://doi.org/10.1017/pab.2018.48 Published online by Cambridge University Press

with $\bar{\sigma}_{VM}$, VF_1, and VF_2 when the attack comes vertically on the osteoderm with no clear influence of either α or λ. The keeled osteoderms score negative *PC1* values, whereas both the spiked and flat osteoderms show rather nil or positive values. Nevertheless, we do not observe any clear pattern distinguishing the square from the rectangular osteoderms along either *PC1* or *PC2* (explaining 5% of the variance).

The Influence of Bone Ornamentation on the Osteoderm Mechanical Response.—In all the osteoderms, the pattern of the von Mises stress is generally similar in either presence or absence of ornamentation (Fig. 5). We notice that both the average von Mises stress ($\bar{\sigma}_{VM}$) and the high-stress volume fractions (VF_1 and VF_2) are higher in the presence of ornamentation. The values of these three mechanical indexes in smoothed and ornamented osteoderms are presented in Table 3, with the corresponding differences in Table 4. The orientation of the attack (parameterized by the angles α and λ) modifies the stress pattern, but only modifies the values of the average von Mises stress to a small extent (Tables 3, 4, Fig. 6).

In general, the average von Mises stress as well as the high-stress volumes (VF_1 and VF_2) are rather higher when the force is applied vertically ($\alpha = 0°$ and $\lambda = 0°$) in both ornamented and smoothed osteoderms. However, the opposite trend is observed in *C. crocodilus* (the osteoderm showing the most pronounced keel in the sample).

The loss of volume due to ornamentation falls between 5% and 15%, which corresponds to a weight loss ranging between 82 and 228 mg per osteoderm (Table 2), assuming a density of $2 g/cm^3$ (compact bone; after Blanton and Biggs 1968). This weight loss depends directly on the degree of ornamentation and is relative to an osteoderm whose size is equivalent to the *C. crocodilus* specimen (scale reference; 27.8 mm [L_y], 18.2 mm [L_x], 4.6 mm [L_z]; Alligatoridae; Table 2). As an *Alligator mississippiensis* adult specimen (Alligatoridae) carries about 70 osteoderms on its dorsal shield (after Sun and Chen, 2013), the corresponding estimated total weight loss due to bone ornamentation should be between 6 and 16 g for any crocodilian presenting a similar dorsal shield and a global size equal to that of *C. crocodilus* (between 2 and 2.5 m; after Groombridge 1987). This value shall be at best doubled (32 g) for an adult *Osteolaemus tetraspis* (Crocodylidae), which shows a similar size but possesses ventral and appendicular osteoderms (Trutnau and Sommerlad 2006).

Discussion

Limits of the Study.—The crocodilian osteoderms are complex mechanical structures that were simplified in this preliminary study. The osteoderms were assumed to be made of a homogeneous and isotropic linearly elastic material. However, these hypotheses can be questioned and will be discussed in this section.

First, the degree of mineralization of the osteoderms is heterogeneous and is noticeably higher in the central keel (when present; Sun and Chen 2013). Moreover, ornamented osteoderms may be composed of different types of bone with both a variable porosity and different collagen fiber orientations (i.e., woven bone, parallel fibered, and lamellar; Burns et al. 2013). Sun and Chen (2013) have performed an extensive experimental analysis through nanoindentation and compressive tests on alligator osteoderms. Their results show that the elastic modulus is heterogeneous (nanoindentation tests provided average elastic moduli of about 20 and 13 GPa in the dorsal and ventral regions, respectively) and anisotropic (compressive tests provided average elastic moduli on the order of 1 GPa, slightly larger in horizontal than in vertical specimens, respectively). The reference Young's modulus of 10 GPa used in this study is coherent with the nanoindentation moduli reported in Sun and Chen (2013: Table 2) after taking into account the porosity of the osteoderm. Indeed, we did not explicitly model the porous microstructure of the core of the osteoderm, and therefore the Young's modulus used in our study (homogeneous throughout the osteoderm) is meant to be an average value accounting for both the solid matrix and the porosity. Nevertheless, in view of the uncertainty affecting the actual value of the Young's modulus, we performed a parametric analysis suggesting

https://doi.org/10.1017/pab.2018.48 Published online by Cambridge University Press

https://doi.org/10.1017/pab.2018.48 Published online by Cambridge University Press

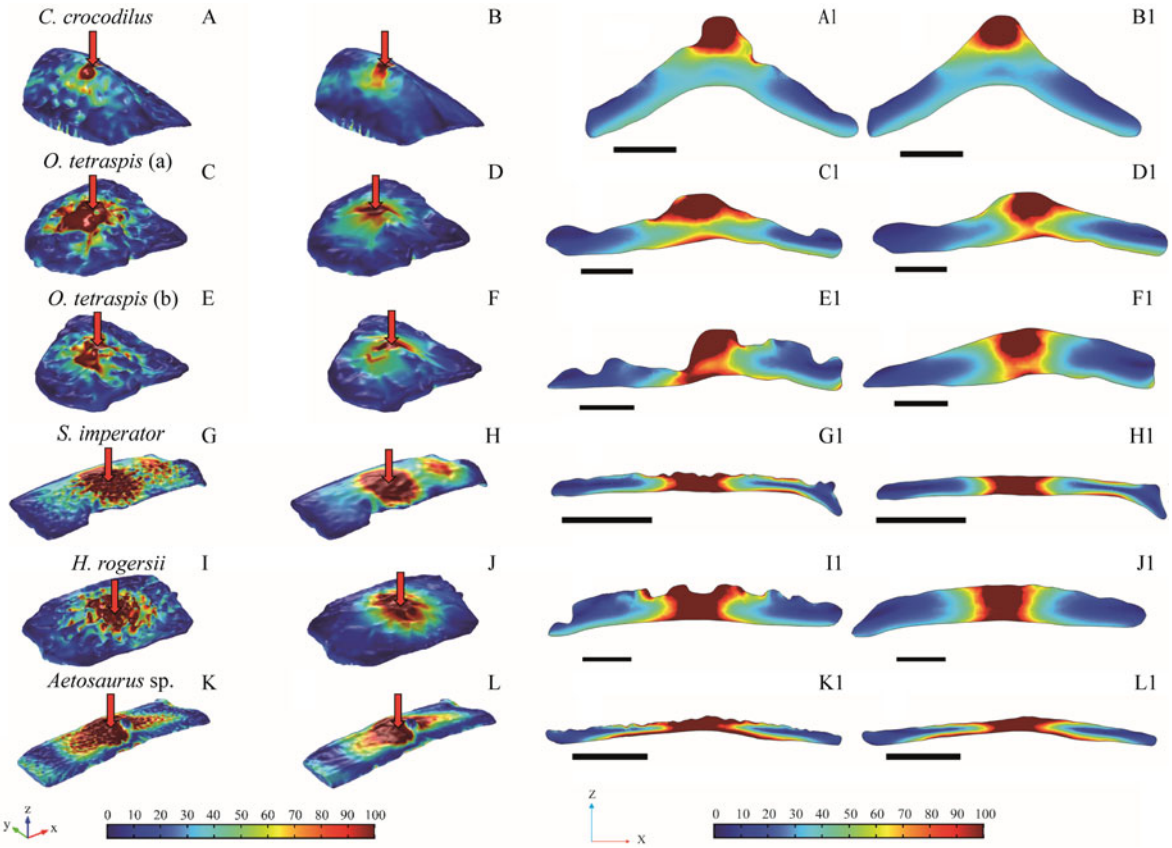


FIGURE 5. von Mises stress in the 3D-modeled osteoderms (in MPa). A, Ornamented osteoderm of *Caiman crocodilus*; A1, view of the mid-osteoderm transversal cross section. Scale bar, 4mm. B, Smoothed osteoderm of *C. crocodilus*; B1, view of the mid-osteoderm transversal cross section. Scale bar, 4 mm. C, Ornamented osteoderm of *Osteolaemus tetraspis* (MNHN-AC.1991.4488a); C1, view of the mid-osteoderm transversal cross section. Scale bar, 4 mm. D, Smoothed osteoderm of *O. tetraspis* (MNHN-AC.1991.4488a); D1, view of the mid-osteoderm transversal cross section. Scale bar, 4 mm. E, Ornamented osteoderm of *O. tetraspis* (MNHN-AC.1991.4488b); E1, view of the mid-osteoderm transversal cross section. Scale bar, 4 mm. F, Smoothed osteoderm of *O. tetraspis* (MNHN-AC.1991.4488b); F1, view of the mid-osteoderm transversal cross section. Scale bar, 4 mm. G, Ornamented osteoderm of *Sarcosuchus imperator*; G1, view of the mid-osteoderm transversal cross section. Scale bar, 10 mm. H, Smoothed osteoderm of *S. imperator*; H1, view of the mid-osteoderm transversal cross section. Scale bar, 10 mm. I, Ornamented osteoderm of *Hyposaurus rogersii*; I1, view of the mid-osteoderm transversal cross section. Scale bar, 4 mm. J, Smoothed osteoderm of *H. rogersii*; J1, view of the mid-osteoderm transversal cross section. Scale bar, 4 mm. K, Ornamented osteoderm of *Aetosaurus* sp.; K1, view of the mid-osteoderm transversal cross section. Scale bar, 10 mm. L, Smoothed osteoderm of *Aetosaurus* sp.; L1, view of the mid-osteoderm transversal cross section. Scale bar, 10 mm. X, transversal axis; Y, longitudinal axis; Z, vertical axis. All plots refer to (α, λ) = (0°, 0°). Color scale: 0 (blue; light gray) to 100 MPa (red; dark gray).

TABLE 4. Differences between the mechanical indexes of the ornamented and smoothed osteoderms (positive values indicate that the index is higher in the actual osteoderm) for each loading condition (α, λ) and on average. See text for details. *Osteolaemus tetraspis* (a), MNHN-AC.1991.4488a; (b), MNHN-AC.1991.4488b.

Caiman crocodilus		Difference		
λ (°)	α (°)	$\Delta\bar{\sigma}_{VM}$ (MPa)	ΔVF_1 (–)	ΔVF_2 (–)
0	0	2.59	0.2%	1.0%
0	–45	3.41	0.9%	3.8%
0	45	3.12	0.4%	3.1%
90	–45	2.92	0.2%	0.4%
90	45	1.70	0.2%	1.7%
Average		2.75	0.4%	2.0%
Osteolaemus tetraspis (a)		Difference		
λ (°)	α (°)	$\Delta\bar{\sigma}_{VM}$ (MPa)	ΔVF_1 (–)	ΔVF_2 (–)
0	0	5.33	1.5%	6.3%
0	–45	3.22	0.5%	3.3%
0	45	6.97	2.2%	7.6%
90	–45	4.75	0.7%	4.6%
90	45	5.06	0.9%	4.8%
Average		5.07	1.2%	5.3%
Osteolaemus tetraspis (b)		Difference		
λ (°)	α (°)	$\Delta\bar{\sigma}_{VM}$ (MPa)	ΔVF_1 (–)	ΔVF_2 (–)
0	0	2.51	0.5%	2.5%
0	–45	3.14	0.7%	3.0%
0	45	2.84	0.7%	2.3%
90	–45	3.14	0.8%	1.8%
90	45	2.31	0.3%	1.7%
Average		2.79	0.6%	2.3%
Sarcosuchus imperator		Difference		
λ (°)	α (°)	$\Delta\bar{\sigma}_{VM}$ (MPa)	ΔVF_1 (–)	ΔVF_2 (–)
0	0	3.89	1.0%	2.3%
0	–45	3.77	0.9%	2.3%
0	45	4.10	0.8%	4.6%
90	–45	3.50	1.1%	2.6%
90	45	2.96	0.9%	1.7%
Average		3.64	0.9%	2.7%
Hyposaurus rogersii		Difference		
λ (°)	α (°)	$\Delta\bar{\sigma}_{VM}$ (MPa)	ΔVF_1 (–)	ΔVF_2 (–)
0	0	7.72	2.7%	5.3%
0	–45	6.51	1.5%	5.8%
0	45	5.91	1.8%	4.7%
90	–45	6.02	1.8%	4.3%
90	45	6.09	1.6%	4.7%
Average		6.45	1.9%	5.0%
Aetosaurus sp.		Difference		
λ (°)	α (°)	$\Delta\bar{\sigma}_{VM}$ (MPa)	ΔVF_1 (–)	ΔVF_2 (–)
0	0	6.98	3.2%	4.2%
0	–45	6.94	2.7%	4.8%
0	45	5.57	1.8%	4.1%
90	–45	5.47	1.6%	3.7%
90	45	5.70	1.7%	4.6%
Average		6.13	2.2%	4.3%

https://doi.org/10.1017/pab.2018.48 Published online by Cambridge University Press

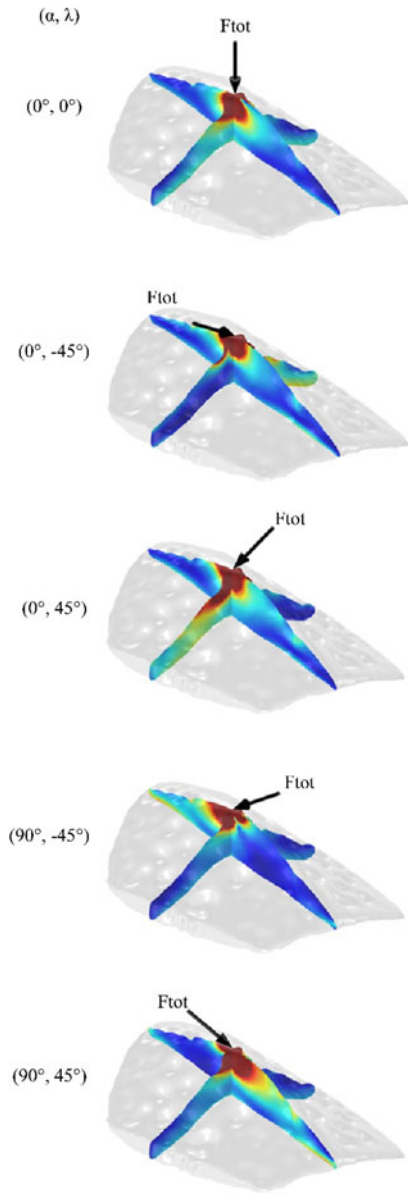


FIGURE 6. von Mises stress in *Caiman crocodilus* osteoderm presented in both longitudinal and transversal cross sections for different loading conditions parameterized by the pair of angles (α, λ). Color scale: 0 (blue; light gray) to 100 MPa (red; dark gray).

that this value has no significant influence on the stress distribution or on the mechanical strength of the osteoderm (Figs. 2A and 3B). In the end, as the same simplifying hypotheses have been made for both the actual and smoothed osteoderm models, it seems reasonable to assume that they will not strongly affect our comparative study. Accounting for the porous structure (i.e., pore size and density) of the osteoderm as well as for the heterogeneity and anisotropy of its elastic properties would require a detailed description of osteoderm microstructure that was not available in this study and will be undertaken in a future work. Indeed, the average Young's modulus is a good approximation of the resulting biomechanical properties, but it cannot fully replicate the morphological differences within the osteoderm.

The attack of a predator was modeled through a force applied on a small part of the top surface of the osteoderm. While considering a variable orientation of this force (from −45° to 45° in two orthogonal planes containing the vertical axis), our study does not encompass any possible attack condition or the sliding of the force on the osteoderm surface that may occur in real situations. More realistic loading conditions would also require fine-tuning the force parameters (magnitude, orientation, contact area, etc.) to mimic the typical attack conditions of the actual predators of each species considered in the study.

The presence of the neighboring osteoderms and of the basal tissue was modeled through elastic springs. Although our parametric analysis with respect to the number of neighboring osteoderms (N) has shown a negligible effect of this parameter, our approach cannot take into account the friction possibly occurring between adjacent osteoderms. Moreover, modeling the basal tissue as vertical springs also neglects possible sliding effects in the horizontal plane. These simplifications do require further attention and will be addressed in future work.

Because the smoothed osteoderms are modeled by considering a quasi-convex fictive envelope joining the top of the ridges ($SoV > RoV$), this model is not suitable to assess the influence of bone ornamentation when this latter is not set up by resorption but only by a differential apposition, such as in temnospondyls, lepospondyls, and placoderms (Witzmann 2009; Buffrénil et al. 2016). In this case, smoothed 3D models could be built by creating the apical bone surface in a different way, for example, by averaging the position of the mesh between the bottom of the pits and the

https://doi.org/10.1017/pab.2018.48 Published online by Cambridge University Press

top of the crests if we consider that the differential apposition consists of consecutive local growth variations resulting in a field of pits and crests.

The Mechanical Effects of the Osteoderm Ornamentation.—Comparing the results obtained for the actual and smoothed osteoderms, it is apparent that the ornamentation has a limited effect on the overall mechanical response of the osteoderm. Indeed, the global mechanical indexes considered in this study (average von Mises stress and high-stress regions) are slightly affected by the ornamentation (see Table 4). The average von Mises stress is higher in the ornamented osteoderms, resulting in an increase of the average von Mises stress of between 10% and 20%. The augmentation in average von Mises stress seems to correlate negatively with the volume difference between actual and smoothed osteoderms (quantified by the index *LV*). Thus, larger differences in $\Delta\bar{\sigma}_{VM}$ (Table 4) are observed in the osteoderms with more pronounced ornamentation (Table 1), namely *H. rogersii* and *O. tetraspis* (MNHN-AC.1991.4488a). However, small differences are observed in *O. tetraspis* (MNHN-AC.1991.4488b), despite its high *LV*. This is likely due to the fact that ornamentation of this sample is mainly located in regions that are not highly stressed.

Concerning the high-stress volume fractions, a similar trend is observed. Critical regions (VF_1 and VF_2; Table 3) are larger in ornamented osteoderms than in their smoothed counterparts, the larger differences (ΔVF_1 and ΔVF_2; Table 4) being observed in osteoderms with more pronounced ornamentation. However, in all cases, the values of ΔVF_1 and ΔVF_2 are on the order of a few percent, proving that the ornamentation does not significantly modify the extent of the critical regions.

In summary, although ornamentation leads to an increased average von Mises stress in the osteoderm, it has quite limited effects on the extent of the highly stressed regions and therefore on the strength of the osteoderms. Nevertheless, this conclusion relies only on global parameters and neglects localization phenomena that are often critical in determining mechanical strength. Actually, stress concentration can be observed close to the pits and ridges of ornamented osteoderms, which may promote crack initiation and propagation and eventually threaten the structural integrity of the osteoderm. This process cannot be described by our model and would require a more detailed analysis accounting for damage and fracture mechanics.

The Influence of the Osteoderm Global Morphology on the von Mises Stress.—The PCA performed using the different variables that quantify the osteoderm mechanical response to an apical external attack ($\bar{\sigma}_{VM}$, VF_1, and VF_2; Fig. 4) reveals that the keeled osteoderms (*C. crocodilus*, *O. tetraspis*) globally have lower stress scores than both the flat and spiked osteoderms (*H. rogersii*, *S. imperator*, *Aetosaurus* sp.), irrespective of their square or rectangular shape. These results somewhat confirm that the presence of a central keel improves the osteoderm strengthening (Sun and Chen 2013). Furthermore, contrary to all other sampled osteoderms, the specimen that shows the more pronounced central keel (*C. crocodilus*; Fig. 5) does have a lower von Mises stress score when the attack is vertical ($\alpha = 0°$ and $\lambda = 0°$; Table 3). The fact that the average von Mises stress in *C. crocodilus* is smaller in case of a vertical force suggests that the morphology of this osteoderm is optimized to withstand this type of attack. Eventually, as evidenced by the parametric analyses, the number of neighboring osteoderms has a negligible influence on the von Mises stress in the impacted osteoderm; therefore, we assume that the relative location of each osteoderm on the body should not have a significant influence on its own mechanical response.

According to previous studies (Sun and Chen 2013; Chen et al. 2014), the presence of pores due to osteoclast activity in the core of the osteoderms tends to enhance the bending stiffness and energy absorption ability with reduced weight. Concerning the ornamentation of the pseudosuchian osteoderms due to superficial osteoclast activity, our results point out that this pattern of pits and grooves tends to slightly increase the local stress values when enduring an external attack but without serious consequence to the global stress pattern (Table 4).

The Role of the Crocodylomorph Ornamented Osteoderms in Adaptative Functions.—The results

https://doi.org/10.1017/pab.2018.48 Published online by Cambridge University Press

discussed earlier emphasize that the presence of apical ornamentation on the pseudosuchian osteoderms does not strongly modify their mechanical response (contra Coldiron 1974) but could rather represent a trade-off between the maintaining of bone strength and the release of mineral components through superficial bone resorption. The direct physical consequence of this mass release either on buoyancy or on any swimming or locomotion performance is of course negligible, as the estimated resulting weight loss is on the order of a few tens of grams for an animal weighting several tens of kilograms (*C. crocodilus*; Staton and Dixon 1975). Nonetheless, this recurrent mineral release (with a high proportion of calcium and phosphor) may possibly answer various physiological needs involving muscle activity (Ca^{2+}), egg shelling (Ca^{2+}; Dacke et al. 2015), ATP synthesis ($PO4^{2}$; Mg^{2+}). Indeed, the pit resorption followed by secondary bone deposition on the pit bottoms is a recurrent process along the crocodylomorph lifetime (Buffrénil 1982; Buffrénil et al. 2015) and may therefore be involved in phosphocalcic homeostasis like any other type of bone remodeling. Moreover, with regard to the yet to be assessed correlation of the increase in the bone ornamentation excavation with the crocodylomorph transition to the ectothermic amphibious lifestyle in the Early Jurassic (Clarac et al. 2017a), it is probable that the bone ornamentation has been involved in physiological adaptations in the evolution of this taxon. In this regard, several authors assessed that the neosuchian, and by extension the teleosaurid, ornamented osteoderms (here represented by *O. tetraspis*, *C. crocodilus*, *S. imperator*, *H. rogersii*) were involved both in the heat transfers during basking (Seidel 1979; Farlow et al. 2010) and in the respiratory acidosis buffering due to lactate accumulation during prolonged apnea (Jackson et al. 2003). Both of these hypotheses rely on the fact that the crocodilian osteoderms provide vascular clusters in a skin that is almost free from vascularization, as shown in Clarac et al. (2018). As detailed in this recent study, the superficial excavation of the bone ornamentation leads to extension of the core osteoderm vessel proliferation to the apical surface, while releasing bone calcium and carbonates that can also contribute to acidosis buffering by respectively complexing with the plasma lactate and increasing the plasma pH (Jackson et al. 2003). Because only the small extant neosuchian species such as *C. crocodilus* still endure predation once they reach maturity (*Panthera onca*; Da Silveira et al. 2010; Azevedo et al. 2011), whereas all the larger species are apex predators once they reach adult size (Trutnau and Sommerlad 2006), we may thus assume that the continuing presence of the dorsal shield in neosuchians may not be due to a function for protection against predators but rather to physiological roles. Therefore, we hypothesize that the adaptative function of bone ornamentation in both the neosuchians and teleosaurids should be to grow a superficial cluster of blood vessels alternatively involved in heat transfers (when emerged or semi-emerged) and acidosis buffering (when submerged). The whole bone remodeling process that drives the genesis and the ontogenetic modifications of the bone ornamentation would thus allow the emergence of physiological functions without involving detrimental consequences to the osteoderm mechanical response.

Unlike the neosuchians, the Triassic pseudosuchians are assumed to be both terrestrial and endothermic (Irmis et al. 2013; Nesbitt et al. 2013; Legendre et al. 2016). Consequently, neither of the above mentioned hypotheses concerning the adaptative physiological implications of the ornamented osteoderms (heat transfers and respiratory acidosis buffering during prolonged apnea) is suitable to explain their function in Triassic pseudosuchians such as the aetosaurs. However, depending on the phylogenetic and paleogeographic context, the aetosaurs may have adopted a vegetarian (Walker 1961; Parrish 1994; Heckert and Lucas 2000) and/or an insectivorous diet (Small 2002; Desojo and Vizcaíno 2009), and they must have experienced the predation of giant terrestrial predators such as rauisuchians (Dzik and Sulej 2007; Nesbitt et al. 2013). In this regard, the aetosaur ornamented dermal shield would have played a role in body protection, although this assumption contradicts the fact that our sampled aetosaur osteoderm experienced more stress than the rest of the sample

https://doi.org/10.1017/pab.2018.48 Published online by Cambridge University Press

when enduring an external attack. Nonetheless, because our sample includes only one aetosaur osteoderm, our result cannot be taken for a general model that would be representative of the entire group. Therefore, no interpretation of the function of the aetosaur ornamented osteoderms can be considered before further investigations are made. Until then, we may simply hypothesize that the morphology and the resulting role of the aetosaur ornamented osteoderm shield may be dependent on both the phylogeny and the taxa's paleogeographic location within the Pangaea (Desojo et al. 2013).

Acknowledgments

We would like to thank the paleontology and comparative anatomy collection managers for giving us access to the specimens: S. Bailon, R. Allain, N. Jalil, D. Germain, J. S. Steyer (Muséum National d'Histoire Naturelle); C. Mehling and M. Norell (American Museum of Natural History). We also send our respectful regards to the UMS 2700 (Muséum National d'Histoire Naturelle/Centre National de la Recherche Scientifique) for the access to the 3D scanner. Finally, we acknowledge A. Evin (Centre National de la Recherche Scientifique, Institut des Sciences de l'Evolution, Montpellier) for her advice concerning morphometrics. No special funding was obtained to perform this investigation.

Literature Cited

Acrai, B., and H. D. Wagner. 2013. Micro-structure and mechanical properties of the turtle carapace as a biological composite shield. Acta Biomaterialia 9:5890–5902.

Akhtar, R., M. J. Sherratt, J. Kennedy Cruickshank, and B. Derby. 2011. Characterizing the elastic properties of tissues. Materials Today 14:96–105.

Anjan, B., and S. Bhullar. 2008. Osteoderms of the California legless lizard *Anniella* (Squamata: Anguidae) and their relevance for considerations of miniaturization. Copeia 4:785–793.

Azevedo, F. C. C., and L. M. Verdade. 2011. Predator–prey interactions: jaguar predation on caiman in a floodplain forest. Journal of Zoology 286:200–207.

Benton, M. J, and A. D. Walker. 2002. *Erpetosuchus*, a crocodile-like basal archosaur from the Late Triassic of Elgin, Scotland. Zoological Journal of the Linnean Society 136:25–47.

Blanton, P. L., and N. L. Biggs. 1968. Density of fresh and embalmed human compact and cancellous bone. American Journal of Physiological Anthropology 29:39–44.

Bochaton, C., V. de Buffrénil, M. Lemoine, S. Bailon, and Y. Ineich. 2013. Body location and tail regeneration effects on osteoderms morphology—are they useful tools for systematic, paleontology, and skeletochronology in diploglossine lizards (Squamata, Anguidae)? Journal of Morphology 276:1333–1344.

Broeckhoven, C., G. Diedericks, and P. L. F. N. Mouton. 2015. What doesn't kill you might make you stronger: functional basis for variation in body armour. Journal of Animal Ecology 84:1213–1221.

Broin, F., and P. Taquet. 1966. Découverte d'un crocodilien nouveau dans le Crétacé inférieur du Sahara (Discovery of a new crocodilian in the lower Cretaceous of the Sahara). Comptes Rendus de l'Académie des Sciences, Paris, série D 262: 2326–2329.

Buffrénil, V. de. 1982. Morphogenesis of bone ornamentation in extant and extinct crocodilians. Zoomorphology 99:155–166.

Buffrénil, V. de, F. Clarac, M. Fau, S. Martin, B. Martin, E. Pellé, and M. Laurin. 2015. Differentiation and growth of bone ornamentation in vertebrates: a comparative histological study among the Crocodylomorpha. Journal of Morphology 21:1–21.

Buffrénil, V. de, F. Clarac, A. Canoville, and M. Laurin. 2016. Comparative data on the differentiation and growth of bone ornamentation in gnathostomes (Chordata: Vertebrata). Journal of Morphology 277:634–670.

Burdak, V. D. 1986. Fonction de protection et fonction de dissimulation du squelette externe. *In* F. J. Meunier and J. Y. Sire, eds. Morphologie fonctionnelle du tégument écailleux des poissons. Société Française d'Ichtyologie 10(3):31–88. Paris, France.

Burns, M. E., M. K. Vickaryous, and P. J Currie. 2013. Histological variability in fossil and recent alligatoroid osteoderms: systematic and functional implications. Journal of Morphology 274:676–686.

Bystrow, A. P. 1935. Morphologische Untersuchungen der Deckknochen des Schädels der Wirbeltiere. I. Mitteilung—Schädel der Stegocephalen. Acta Zoologica Stockholm 16:65–141.

Cerda, I. A., and J. B. Desojo. 2011. Dermal armour histology of aetosaurs (Archosauria: Pseudosuchia), from the Upper Triassic of Argentina and Brazil. Lethaia 44:417–428.

Cerda, I. A., J. B. Desojo, T. M. Scheyer, and C. L. Schultz. 2013. Osteoderm microstructure of "rauisuchian" archosaurs from South America. Geobios 46:273–283.

Chen, I. H., J. H. Kiang, V. Correa, M. I. Lopeza, P. Y. Chen, J. McKittrick, and M. A. Meyers. 2011. Armadillo armor: mechanical testing and micro-structural evaluation. Journal of the Mechanical Behavior of Biomedical Materials 4:713–722.

Chen, I. H., W. Yang, and M. A. Meyers. 2014. Alligator osteoderms: mechanical behavior and hierarchical structure. Material Science Engineering C 35:441–448.

——. 2015. Leatherback sea turtle shell: a tough and flexible biological design. Acta Biomaterialia 28:2–12.

Clarac, F., T. Souter, R. Cornette, J. Cubo, and V. de Buffrénil. 2015. A quantitative assessment of bone area increase due to ornamentation in the Crocodylia. Journal of Morphology 276:1183–1192.

Clarac, F., V. de Buffrénil, C. A. Brochu, and J. Cubo. 2017a. The evolution of bone ornamentation in Pseudosuchia: morphological constraints versus ecological adaptation. Biological Journal of the Linnean Society 121:395–408.

Clarac, F., F. Goussard, L. Teresi, V. de Buffrénil, and V. Sansalone. 2017b. Do the ornamented osteoderms influence the heat conduction through the skin? A finite element analysis in Crocodylomorpha. Journal of Thermal Biology 69:39–53.

Clarac, F., V. de Buffrénil, J. Cubo, and A. Quilhac. 2018. Vascularization in ornamented osteoderms: physiological implications in ectothermy and amphibious lifestyle in the crocodylomorphs? Anatomical Record 301:175–183.

Coldiron, R. W. 1974. Possible functions of ornament in the labyrinthodont amphibians. Occasional Papers of the of Museum National History of Kansas 33:1–19.

Cope, E. D. 1861. Recent species of Emydosaurian reptiles represented in the Museum of the Academy. Proceedings of the Academy of Natural Sciences of Philadelphia1860:549–551.

Dacke, C. G., R. M. Elsey, P. L. Trosclair, T. Sugiyama, J. G. Nevarez, and M. H. Schweitzer. 2015. Alligator osteoderms as a source

https://doi.org/10.1017/pab.2018.48 Published online by Cambridge University Press

of labile calcium for eggshell formation. Journal of Zoology 297:255–264.

Da Silveira, R., E. E. Ramalho, J. B. Thorbjarnarson, and W. E. Magnusson. 2010. Depredation by jaguars on caimans and importance of reptiles in the diet of jaguar. Journal of Herpetology 44:418–424.

Desojo, J. B., and S. Vizcaíno. 2009. Jaw biomechanics in the South American aetosaur *Neoaetosauroides engaeus*. Paläontologische Zeitschrift 83:499–510.

Desojo, J. B., A. B. Heckert, J. W. Martz, W. G. Parker, R. R. Schoch, B. J. Small, and T. Sulej. 2013. Aetosauria: a clade of armoured pseudosuchians from the Late Triassic continental beds. *In* S. J. Nesbitt, J. B. Desojo, and R. B. Irmis, eds. Anatomy, phylogeny and palaeobiology of early archosaurs and their kin. Geological Society Special Publication 379:203–239.

Dubansky, B. H., and B. D. Dubansky. 2018. Natural development of dermal ectopic bone in the American alligator (*Alligator mississippiensis*) resembles heterotopic ossification disorders in humans. Anatomical Record 301:56–76.

Du Plessis, A., C. Broeckhoven, I. Yadroitsev, I. Yadroitsava, and S. G. le Roux. 2018. Analyzing nature's protective design: the glyptodont body armor. Journal of the Mechanical Behavior of Biomedical Materials 82:218–223.

Dzik, J., and T. Sulej. 2007. A review of the early Late Triassic Krasiejów biota from Silesia, Poland. Palaeontologia Polonica 64:3–27.

Erickson, G. M., P. M. Gignac, S. J. Steppan, A. K. Lappin, K. A. Vliet, J. D. Brueggen, B. D. Inouye, D. Kledzik, and G. J. W. Webb. 2012. Insights into the ecology and evolutionary success of crocodilians revealed through bite-force and tooth-pressure experimentation. PLoS ONE 7(3):e31781. doi: 10.1371/journal.pone.0031781.

Farlow, J. O., S. Hayashi, and G. J. Tattersall. 2010. Internal vascularity of the dermal plates of *Stegosaurus* (Ornithischia, Thyreophora). Swiss Journal of Geosciences 103:173–185.

Fraas, O. 1877. *Aetosaurus ferratus* Fr. Die gepanzerte Vogel-Echse aus dem Stubensandstein bei Stuttgar. Festschrift zur Feier des 400jährigen Jubiläums der Eberhard-Karls-Universät zu Tübingen, Wurttembergische naturwissenschaftliche jahreshefte 33 (3):1–22.

Gasc, J. P. 1981. Axial musculature B. Crocodilia. *In* C. Gans, and T. S. Parsons, eds. Biology of the Reptilia 11:372–376. London.

Gilbert, S. F., G. A. Loredo, A. Brukman, and A. C. Burke. 2001. Morphogenesis of the turtle shell: the development of a novel structure in tetrapod evolution. Evolution and Development 3:47–58.

Groombridge, B. 1987. The distribution and status of world crocodilians. Pp. 9–21 *in* G. J. W. Webb, S. C. Manolis, and P. J. Whitehead, eds. Wildlife management—crocodiles and alligators. Surrey Beatty and Sons, Chipping Norton, NSW, Australia.

Hammer, Ø., D. A. T. Harper, and P. D. Ryan. 2001. PAST: Paleontological statistics software package for education and data analysis. Palaeontologia Electronica 4(1):9. http://palaeoelectronica.org/2001_1/past/issue1_01.htm.

Heckert, A. B., and S. G. Lucas. 2000. Taxonomy, phylogeny, biostratigraphy, biochronology, paleobiogeography, andevolution of the Late Triassic Aetosauria (Archosauria:Crurotarsi). Zentralblatt für Geologie und Paläontologie 11–12:1539–1587.

Heckert, A. B., C. N. Fraser, and V. P. Schneider. 2017. A new species of *Coahomasuchus* (Archosauria, Aetosauria) from the Upper Triassic Pekin Formation, Deep River Basin, North Carolina. Journal of Paleontology 91:162–178.

Iordansky, N. N. 1973. The skull of the Crocodilia. Pp. 201–262 *in* C. Gans, ed. Biology of the Reptilia. Academic, London.

Irmis, R. B., S. J. Nesbitt, and H. D. Sues. 2013. Early Crocodylomorpha. Geological Society of London Special Publication 379:275–302.

Jackson, D. C. 2000. Living without oxygen: lessons from the freshwater turtle. Comparative Biochemistry and Physiology Part A 125:299–315.

Jackson, D. C., and N. Heisler. 1982. Plasma ion balance in submerged anoxic turtles at 3°C: the role of calcium lactate formation. Respiration Physiology 49:159–174.

Jackson, D. C., Z. Goldberger, S. Visuri, and R. N. Armstrong. 1999. Ionic exchanges of turtle shell *in vitro* and their relevance to shell function in the anoxic turtle. Journal of Experimental Biology 202:503–520.

Jackson, D. C., C. E. Crocker, and G. R. Ultsch. 2000a. Bone and shell contribution to lactic acid buffering of submerged turtles *Chrysemys picta bellii* at 3°C. American Journal of Physiology: Regulatory, Integrative and Comparative Physiology 278:R1964–1571.

Jackson, D. C., A. L. Ramsey, J. M. Paulson, C. E. Crocker, and G. R. Ultsch. 2000b. Lactic acid buffering by bone and shell in anoxic softshell and painted turtles. Physiological and Biochemical Zoology 73:290–297.

Jackson, D. C., D. Andrade, and A. S. Abe. 2003. Lactate sequestration by osteoderms of the broadnose caiman, *Caiman latirostris*, following capture and forced submergence. Journal of Experimental Biology 206:3601–3606.

Kälin, J., 1955. Crocodilia. *In* J. Piveteau, ed. Traité de Paléontologie 5:695–784. Masson et Cie, Paris.

Kot, B. C. W., Z. J. Zhang, A. W. C. Lee, V. Y. F. Leung, and S. N. Fu. 2012. Elastic modulus of muscle and tendon with shear wave ultrasound elastography: variations with different technical settings. PLoS ONE 7(8):e44348. doi: 10.1371/journal.pone.0044348.

Legendre, L., G. Guénard, J. Botha-Brink, and J. Cubo. 2016. Palaeohistological evidence for ancestral high metabolic rate in archosaurs. Systematic Biology 65:989–996.

Linnaeus, Cv. 1758. Amphibia Lacerta. *In* Systema naturae. Tome 1:1057–1058.

Long, R. A., and K. L. Ballew. 1985. Aetosaur dermal armor from the Late Triassic of southwestern North America, with special reference to material from the Chinle Formation of Petrified Forest National Park. *In* E. H. Colbert and R. R. Johnson, eds. The petrified forest through the ages. Museum of Northern Arizona Bulletin 54:45–68. Flagstaff, Ariz.

Main, R. P., Ade. Ricqlès, J. R. Horner, and K. Padian. 2005. The evolution and function of thyreophoran dinosaur scutes: implications for plate function in stegosaurs. Paleobiology 31:291–314.

McKee, C. T., J. A. Last, P. Russell, and C. J. Murphy. 2011. Indentation versus tensile measurements of Young's modulus for soft biological tissues. Tissue Engineering Part B 17:155–164.

Mises, R. von. 1913. Mechanik der festen Körper im plastisch deformablen Zustand. Göttingen Mathematisch-Physikalische Klasse 1:582–592.

Nesbitt, S. J. 2011. The early evolution of archosaurs: relationships and the origin of major clades. Bulletin of the American Museum National History 352:1–292.

Nesbitt, S. J., J. B. Desojo, and R. B. Irmis. 2013. Anatomy, phylogeny and palaeobiology of early archosaurs and their kin. Geological Society of London Special Publication 379:1–7.

Owen, R. 1849. Notes on remains of fossil reptiles discovered by Prof. Henry Rogers of Pennsylvania, U. S., in Greensand formation of New Jersey. Quarterly Journal of the Geological Society of London 5:380–383.

Parrish, J. M. 1994. Cranial osteology of *Longosuchus meadei* and the phylogeny and distribution of the Aetosauria. Journal of Vertebrate Paleontology 14:196–209.

Pithioux, M., P. Lasaygues, and P. Chabrand. 2002. An alternative ultrasonic method for measuring the elastic properties of cortical bone. Journal of Biomechanics 35:961–968.

Ross, F. D., and G. C. Mayer. 1983. On the dorsal armor of the Crocodilia. Pp. 305–331 *in* A. G. J. Rhodin, ed. Advances in herpetology and evolutionary biology. Museum of Comparative Zoology. Cambridge, Mass.

https://doi.org/10.1017/pab.2018.48 Published online by Cambridge University Press

Rinehart, L. F., and S. G. Lucas. 2013. The functional morphology of dermal bone ornamentation in temnospondyl amphibians. *In* L. H. Tanner, J. A. Spielmann, and S. G. Lucas, eds. The Triassic System 61:524–532. New Mexico Museum of Natural History and Science, Albuquerque, N.M.

Scheyer, T. M., and J. B. Desojo. 2011. Palaeohistology and external microanatomy of rauisuchian osteoderms (Archosauria: Pseudosuchia). Palaeontology 54:1289–1302.

Scheyer, T. M., and P. M. Sander. 2004. Histology of ankylosaur osteoderms: implications for systematics and function. Journal of Vertebrate Paleontology 24:874–893.

Scheyer, T. M., M. P. Sander, W. G. Joyce, W. Böhme, and U. Witzel. 2007. A plywood structure in the shell of fossil and living softshelled turtles (Trionychidae) and its evolutionary implications. Organism Diversity and Evolution 7:136–144.

Scheyer, T. M., T. Mörs, and E. Einarsson. 2012. First record of softshelled turtles (Cryptodira, Tryonychidae) from the Late Cretaceous of Europe. Journal of Vertebrate Paleontology 32:1027–1032.

Scheyer, T. M., J. B. Desojo, and I. A. Cerda. 2014. Bone histology of phytosaur, aetosaur, and other archosauriform osteoderms (Eureptilia, Archosauromorpha). Anatomical Record 297:240–260.

Schoch, R. R., and J. B. Desojo. 2016. Cranial anatomy of the aetosaur *Paratypothorax andressorum* from the Upper Triassic of Germany and its bearing on aetosaur phylogeny. Neues Jahrbuch für Geologie und Paläontologie 279:73–95.

Seidel, M. R. 1979. The osteoderms of the American alligator and their functional significance. Herpetologica 35:375–380.

Sereno, P. C., H. C. Larsson, C. A. Sidor, and B. Gado. 2001. The giant crocodyliform *Sarcosuchus* from the Cretaceous of Africa. Science 294:1516–1519.

Small, B. J. 2002. Cranial anatomy of *Desmatosuchus haplocerus* (Reptilia: Archosauria: Stagonolepididae). Zoological Journal of the Linnean Society 136:97–111.

Staton, M. A., and J. R. Dixon. 1975. Studies on dry season biology of *Caiman crocodilus crocodiles* from the Venezuela Llanos. Memoria de la Sociedad de Ciencias Naturales La Salle 101:237–265.

Stocker, M. R., and R. J. Butler. 2013. Phytosauria. *In* S. J. Nesbitt, J. B. Desojo, and R. B. Irmis, eds. Anatomy, phylogeny and palaeobiology of early archosaurs and their kin. Geological Society Special Publication 379:91.

Sun, C. Y., and P. Y. Chen. 2013. Structural design and mechanical behavior of alligator (*Alligator mississippiensis*) osteoderms. Acta Biomaterialia 9:9049–9064.

Trutnau, L., and R. Sommerlad. 2006. Crocodilians their natural history and captive husbandry. Edition Chimaira, Frankfurt am Main, Germany.

Vickaryous, M. K., and B. K. Hall. 2006. Osteoderm morphology and development in the nine-banded armadillo, *Dasypus novemcinctus* (Mammalia, Xenarthra, Cingulata). Journal of Morphology 267:1273–1283.

——. 2008. Development of the dermal skeleton in *Alligator mississippiensis* (Archosauria, Crocodylia) with comments on the homology of osteoderms. Journal of Morphology 269:398–422.

Vickaryous, M. K., and J. Y. Sire. 2009. The integumentary skeleton of tetrapods: origin, evolution and development. Journal of Anatomy 214:441–464.

Walker, A. D. 1961. Triassic reptiles from the Elgin area: *Stagonolepis*, *Dasygnathus* and their allies. Philosophical Transactions of the Royal Society of London B 244:103–204.

Witzmann, F. 2009. Comparative histology of sculptured dermal bones in basal tetrapods, and the implications for the soft tissue dermis. Palaeodiversity 2:233–270.

Wolf, D., D. C. Kalthof, and P. M. Sander. 2012. Osteoderm histology of the Pampatheriidae (Cingulata, Xenarthra, Mammalia): implications for systematics, osteoderm growth, and biomechanical adaptation. Journal of Morphology 273:388–404.

Yang, W., I. H. Chen, B. Gludovatz, E. A. Zimmermann, R. O. Ritchie, and M. A. Meyers. 2013a. Natural flexible dermal armor. Advanced Material 25:31–48.

Yang, W., B. Gludovatz, E. A. Zimmermann, H. A. Bale, R. O. Ritchie, and M. A. Meyers. 2013b. Structure and fracture resistance of alligator gar (*Atractosteus spatula*) armored fish scales. Acta Biomaterialia 9:5876–5889.

Zylberberg, L., and J. Castanet. 1985. New data on the structure and the growth of the osteoderms in the reptile *Anguis fragilis* (Anguidae, Squamata). Journal of Morphology 186:327–342.

https://doi.org/10.1017/pab.2018.48 Published online by Cambridge University Press